DTU Library

Coordinated Voltage Control of a Wind Farm based on Model Predictive Control

Zhao, Haoran; Wu, Qiuwei; Guo, Qinglai; Sun, Hongbin; Huang, Shaojun; Xue, Yusheng

Coordinated Voltage Control of a Wind Farm based on Model Predictive Control

Haoran Zhao, Qiuwei Wu, Qinglai Guo, Hongbin Sun, Shaojun Huang and Yusheng Xue

Abstract—This paper presents an autonomous wind farm voltage controller based on Model Predictive Control (MPC). The reactive power compensation and voltage regulation devices of the wind farm include Static Var Compensators (SVCs), Static Var Generators (SVGs), Wind Turbine Generators (WTGs) and On-Load Tap Changing (OLTC) Transformer, and they are coordinated to keep the voltages of all the buses within the feasible range. Moreover, the reactive power distribution is optimized throughout the wind farm in order to maximize the dynamic reactive power reserve. The sensitivity coefficients are calculated based on an analytical method to improve the computation efficiency and overcome the convergence problem. Two control modes are designed for both voltage violated and normal operation conditions. A wind farm with 20 wind turbines was used to conduct case studies to verify the proposed coordinated voltage control scheme under both normal and disturbance conditions.

Index Terms—Dynamic reactive power reserve, model predictive control, sensitivity coefficient, wind farm, voltage control.

NOMENCLATURE

A. Parameters

1) Wind farm network

N_B Number of buses in wind farm.

Y_bus Admittance matrix of wind farm.

2) WTGs

N_W Number of WTGs.

T_W Time constant of WTGs.

$Q_\mathrm{W}^{\min}, Q_\mathrm{W}^{\max}$ Min. and max. Var capacities of WTGs.

3) SVCs/SVGs

N_S Number of SVCs/SVGs.

T_S Time constant of SVCs/SVGs.

$K_\mathrm{P}, K_\mathrm{I}$ Proportional and Integral gains of PI controller of SVCs/SVGs.

$Q_\mathrm{S}^{\min}, Q_\mathrm{S}^{\max}$ Min. and max. Var capacities of SVCs/SVGs.

4) OLTC

ΔV_tap Voltage change per tap.

V_DB Dead-band of OLTC controller.

T_delay Delay time of OLTC.

5) WFVC

$V_\mathrm{POC}^{\mathrm{ref}}, V_\mathrm{MV}^{\mathrm{ref}}, V_\mathrm{W}^{\mathrm{ref}}$ Voltage references at POC, MV and WTG buses.

$V_\mathrm{POC}^{\mathrm{th}}, V_\mathrm{MV}^{\mathrm{th}}, V_\mathrm{W}^{\mathrm{th}}$ Thresholds of V_POC, V_MV and V_W.

$W_\mathrm{POC}, W_\mathrm{MV}, W_\mathrm{W}$ Weighting factors of voltage deviations at POC, MV and WTG buses.

W_S Weighting factor of Var deviation of SVCs/SVGs.

ΔT_P Prediction period of WFVC.

ΔT_c Control period of WFVC.

T_P Prediction horizon of WFVC.

N_P Prediction steps of WFVC.

N_c Control steps of WFVC.

B. Sets

$\mathcal{N}$ Set of buses in wind farm.

C. Variables

$S, \overline{S}$ Power and its conjugate in complex form.

$V, \overline{V}$ Voltage and its conjugate in complex form.

θ Phase angle of voltage.

$V_\mathrm{POC}, V_\mathrm{MV}, V_\mathrm{W}$ Voltages at POC, MV and WTG buses.

$\Delta V_\mathrm{POC}, \Delta V_\mathrm{MV}, \Delta V_\mathrm{W}$ Voltage changes at POC, MV and WTG buses.

P_W Active power of WTGs.

Q_W Reactive power of WTGs.

$Q_\mathrm{W}^{\mathrm{ref}}$ References of reactive power of WTGs.

$\Delta Q_\mathrm{W}^{\mathrm{ref}}$ References of reactive power change of WTGs.

V_S Voltage at the bus controlled by SVCs/SVGs.

$V_\mathrm{S}^{\mathrm{ref}}$ Reference of voltage at the bus controlled by SVCs/SVGs.

$\Delta V_\mathrm{S}^{\mathrm{ref}}$ Reference of voltage change at the bus controlled by SVCs/SVGs.

ΔV_int Integral of the deviation between $V_\mathrm{S}^{\mathrm{ref}}$ and V_S.

Q_S Reactive power of SVCs/SVGs.

$Q_\mathrm{S}^{\mathrm{ref}}$ Reference reactive power of SVCs/SVGs.

$\Delta Q_\mathrm{S}^{\mathrm{ref}}$ Reference of reactive power change of SVCs/SVGs.

n_tap Tap position of OLTC.

H. Zhao is with Center for Electric Power and Energy (CEE), Department of Electrical Engineering, Technical University of Denmark (DTU), Kgs. Lyngby, 2800 Denmark, and Sino-Danish Center for Education and Research (SDC), Aarhus, 8000 Denmark (e-mail: hzhao@elektro.dtu.dk).

Q. Wu is with Center for Electric and Energy (CEE), Department of Electrical Engineering, Technical University of Denmark (DTU), Kgs. Lyngby, 2800 Denmark, Sino-Danish Center for Education and Research (SDC), Aarhus, 8000 Denmark, and School of Electrical Engineering, Shandong University, China (e-mail: qw@elektro.dtu.dk).

Q. Guo and H. Sun are with Department of Electrical Engineering, Tsinghua University, Beijing, 100084 China (e-mail: guoqinglai@tsinghua.edu.cn; shb@mail.tsinghua.edu.cn).

S. Huang is with Center for Electric Power and Energy (CEE), Department of Electrical Engineering, Technical University of Denmark (DTU), Kgs. Lyngby, 2800 Denmark (e-mail: shuang@elektro.dtu.dk).

Y. Xue is with State Grid Electric Power Research Institute, Nanjing 210003, China (e-mail: xueyusheng@sgepri.sgcc.com.cn).

t_{tri} Trigger time of OLTC.

t_{act} Action time of OLTC.

I. INTRODUCTION

THE increasing penetration of wind power and growing size of the wind farm have big impacts on the system operation and introduce technical challenges to voltage stability [1]. Since large wind farms are mainly located in areas far from load centers, the Short Circuit Ratio (SCR) is small [2], and the grid at the connection point is weak. The voltage fluctuation caused by the intermittent power of the wind farms is quite large. Moreover, the grid disturbance may cause cascading trip of Wind Turbine Generators (WTGs). Therefore, modern wind farms are required to meet more stringent technical requirements of voltage support specified by system operators. The requirements include reactive power capability of the wind farm and voltage operating range at the Point of Connection (POC) [3].

In order to fulfill these requirements, wind farms have a variety of reactive power (Var) or voltage (Volt) regulation devices: Static Var Compensators (SVCs), Static Var Generators (SVGs), On Load Tap Changing (OLTC) Transformer, etc. Besides, with the development of power electronics and control technologies, modern WTGs equipped with power electronic converters (Type 3 and Type 4) can control the reactive power, and participate in the voltage control [4].

Several modes to control the reactive power of a wind farm have been specified by many grid codes which are defined by transmission system operators for wind power integration, including power factor control, reactive power control and voltage control [5]. For the transmission system, the voltage control mode shows superior performance. This paper focuses on the wind farm control under this mode, i.e. the wind farm controls the voltage at the POC specified by the system operator.

Compared with the voltage control of a conventional power plant, two issues shall be addressed for the wind farm voltage control. The first issue is related to the collector system of the wind farm. This collector system connects a large number of WTGs by several Medium Voltage (MV) feeders. These feeders are quite long and their X/R ratio is low ($X/R \leq 1$). Therefore, the voltage change along the feeder should not be neglected. The voltages of WTGs at the end of the feeders may be close to their limits and the WTGs have a risk of being tripped. The second issue is related to the coordination among different voltage regulation devices. The dynamic response of these devices are different. For SVCs/SVGs, the response is quite fast, whose time constant is within milliseconds ($50 \sim 200\,\text{ms}$ for SVCs and $20 \sim 100\,\text{ms}$ for SVGs) [6]. For WTGs, the response time is in the range of $1 \sim 10\,\text{s}$ [7]. For the OLTC, the time required to move from one tap position to another largely depends on the tap changer design, which may vary from a few seconds to several minutes [8]. Without proper coordination among these devices, conflicts may occur between the control performances and objectives.

Several control strategies have been designed for the Wind Farm Voltage Controller (WFVC). In [9]–[11], the total required reactive power reference is calculated according to the voltage at the POC and then dispatched to all WTGs based on proportional distribution of the maximum or available reactive power. This method is easy to be implemented. However, the voltages of WTG buses are not taken into account. In [12], the reactive power is optimally distributed. The detailed model of the wind farm collector system is used to calculate the sensitivity coefficients. However, this optimal control is only based on the current status. The fast and slow devices in a longer period are not coordinated. Besides, the discrete variables, such as OLTC tap position, is not considered.

Recently, Model Predictive Control (MPC) has attracted more and more attention. It uses the receding horizon principle, such that a finite-horizon optimal control problem is solved over a fixed interval of time. It is suitable for the coordinated control among various Var devices in the wind farm.

The main contribution of this paper is the MPC based WFVC design, which aims to maintain all the bus voltages within their feasible range and maximize the fast dynamic Var reserve. The calculation of the sensitivity coefficients is based on an analytical method to improve the computation efficiency and overcome the possible convergence problem. Moreover, the OLTC is incorporated into the MPC without changing the control structure.

The paper is organized as follows. Section II presents the concept of the proposed WFVC. The sensitivity coefficient calculation is introduced in Sections III. The discrete modeling of the Var/Volt devices are described in Section IV and Section V. Section VI explains the formulation of the MPC problem. Case studies are presented and discussed in Section VII, followed by conclusions.

II. MPC BASED WFVC

The configuration of a wind farm and the structure of the proposed MPC based WFVC are illustrated in Fig. 1 and Fig. 2, respectively. The buses within the wind farm include a bus at the POC (corresponding to the High Voltage (HV) side of the main substation transformer), a bus at the MV side of the main substation transformer and buses of WTGs.
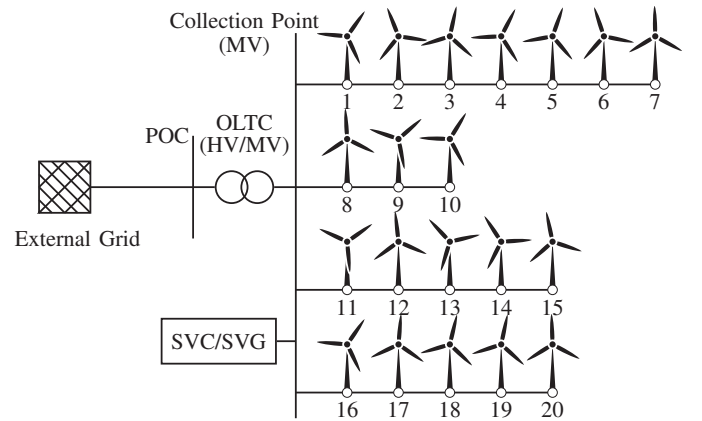

Fig. 1. Configuration of a wind farm.

The MPC controller of the WFVC has two control modes according to different operating conditions: (1) corrective
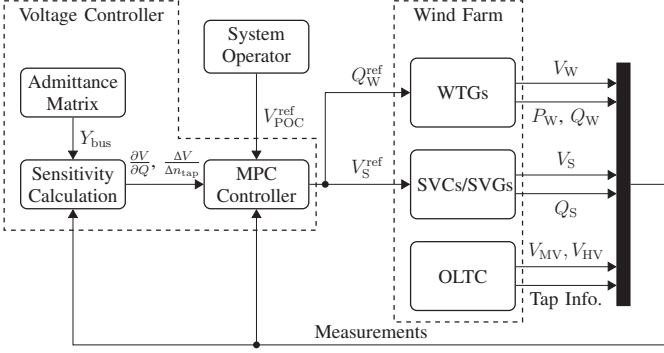
Fig. 2. Voltage control structure of a wind farm.

control mode, it can be considered as emergency control which aims to correct any bus voltage of the wind farm violating the limits; (2) preventive control mode, which aims to maximize the fast Var reserve to handle the potential disturbance in the future, and further minimize the voltage deviation at the POC V_{POC} from its reference value $V_{\text{POC}}^{\text{ref}}$ from the system operator. More details of these two control modes are described in Section VI. The MPC controller determines the regulation commands for all WTGs ($Q_{\text{W}}^{\text{ref}}$) and SVCs/SVGs ($V_{\text{S}}^{\text{ref}}$).

The modern WTGs are able to track the Var set point $Q_{\text{W}}^{\text{ref}}$ by upgrading the converters constant-Q control loop. Due to the large number, the contribution of WTGs to the voltage control is considerable. Besides, the WTGs are distributed along the feeders and it is possible to control the voltages of different buses all over the wind farm.

The SVCs/SVGs can operate under either constant-V mode or constant-Q mode. It is easier to be coordinated with the WTGs by adopting the constant-Q mode. However, if the voltage at the SVC's controlled bus violates the limits, the SVCs/SVGs can not provide dynamic Var support to regulate the voltage of the controlled bus (POC in this study) in time. In [12], a control algorithm combining the constant-V and constant-Q was developed. The control mode of SVCs/SVGs switches according to the voltage of the controlled bus. In order to reduce the control complexity, the constant-V mode is adopted in this study. Based on the prediction model and $V_{\text{S}}^{\text{ref}}$, the equivalent Var reference of SVCs/SVGs, $Q_{\text{S}}^{\text{ref}}$, can be calculated and coordinated with the WTGs.

The OLTC refers to the HV/MV transformer located at the main substation of the wind farm. Since the sampling period of the WFVC is normally in seconds, in order to detect the voltage violation between two sequential control actions, the automatic tap controller of the OLTC is included in this study. As shown in Fig. 2, the MPC controller doesn't control the tap changer directly. The relevant information, such as trigger time and tap position, will be sent to the MPC controller. More details of the implementation of the OLTC in the MPC is described in Section V.

Due to the low X/R ratio of the collector system, the impact of the active power change ΔP_{W} on the voltage variation can not be neglected. P_{W} is considered as a measurable disturbance and the prediction horizon of the MPC is based on the power forecast. Due to the large rotor inertia constant

($3 \sim 5\,\text{s}$), the modern WTGs act as a low pass filter and smooth the output power to some extent [13]. In this study, the persistence assumption is applied for the short-period prediction. Thus, the Var outputs (Q_{W}, Q_{S}) and the tap change of OLTC (n_{tap}) play the major role in the voltage change. The corresponding sensitivity coefficients shall be calculated and sent to the MPC controller. Since the sensitivity coefficients vary with the operating points, these values shall be updated for each control step.

III. SENSITIVITY COEFFICIENT CALCULATION

The conventional calculation method of the sensitivity coefficients is through an updated Jacobian matrix derived from the load flow. However, the main disadvantage of such a method is that, the Jacobian matrix needs to be rebuilt and inversed for every change of the operation conditions in the network. This procedure creates non-trivial computation constraints for the implementation of real-time centralized or decentralized controllers. Besides, the Jacobian-based method uses Newton-Raphson (NR) method for the load-flow solution. However, the low X/R ratio of the wind farm network makes the NR method sometimes fail to converge in solving the load-flow problem [14], [15].

In order to improve the computation efficiency, an analytical computation method for calculating the sensitivity coefficients was developed in [16]. It was initially applied in the radial distribution system. Since the collector system of the wind farm has a similar network topology, this method is adopted in this paper.

A. Sensitivity coefficient to reactive power

Consider a wind farm with N_{B} buses, define $\mathcal{N}$ as the set of all buses $\mathcal{N} = \{1, 2, \cdots N_{\text{B}}\}$. It is assumed that the PQ injections at each bus are constant and their dependences on the voltage are ignored [16]. For each separate perturbation of nodal power injections, the power set points of WTGs or SVCs/SVGs at other buses don't change.

The relation between the power injection S and voltage V (both in complex form) is

$$\overline{S_i} = \overline{V_i} \sum_{j \in \mathcal{N}} (Y_{\text{bus}}(i,j)V_j), \tag{1}$$

where i and j are the bus indexes, Y_{bus} is the admittance matrix, $\overline{S}$ and $\overline{V}$ are the conjugates of S and V, respectively.

The partial derivatives of the voltage at Bus $i \in \mathcal{N}$ with respect to reactive power Q_l at Bus $l \in \mathcal{N}$ satisfy the following equations,

$$\frac{\partial \overline{S_i}}{\partial Q_l} = \frac{\partial \{P_i - \text{j}Q_i\}}{\partial Q_l} = \frac{\partial \overline{V_i}}{\partial Q_l} \sum_{j \in \mathcal{N}} Y_{\text{bus}}(i,j)V_j + \tag{2}$$

$$\overline{V_i} \sum_{j \in \mathcal{N}} Y_{\text{bus}}(i,j)\frac{\partial V_j}{\partial Q_l} = \begin{cases} -\text{j}1, & \text{if } i = l. \\ 0, & \text{else.} \end{cases}$$

Equations (2) is linear to the unknown variables $\frac{\partial V_i}{\partial Q_l}$, $\frac{\partial \overline{V_i}}{\partial Q_l}$. According to the theorem in [16], (2) has a unique solution for radial electrical networks.

Once $\frac{\partial V_i}{\partial Q_l}$, $\frac{\partial \overline{V_i}}{\partial Q_l}$ are obtained, the partial derivatives of the voltage magnitude $\frac{\partial |V_i|}{Q_l}$ can be calculated by,

$$\frac{\partial |V_i|}{\partial Q_l} = \frac{1}{|V_i|}\text{Re}(\overline{V_i}\frac{\partial V_i}{\partial Q_l}). \tag{3}$$

B. Sensitivity coefficient to tap position

The analytical expressions of the voltage sensitivity coefficients with respect to tap positions of a transformer is introduced in this subsection. The power injections at the buses are assumed to be constant and their dependences on the voltage are ignored.

Define $V_l = |V_l|e^{j\theta_l}$ for all buses l. θ is the phase angle of the voltage. The tap changer is located at Bus k. For a bus $i \in \mathcal{N}$, the partial derivatives with respect to the voltage magnitude $|V_k|$ of the Bus k are

$$-\overline{V_i}Y_{\text{bus}}(i,k)e^{j\theta_k} = \overline{W_{ik}}\sum_{j\in\mathcal{N}}(Y_{\text{bus}}(i,j)V_j) + \overline{V_i}\sum_{j\in\mathcal{N}}Y_{\text{bus}}(i,j)W_{jk}, \tag{4}$$

where

$$W_{ik} \triangleq \frac{\partial V_i}{\partial |V_k|} = (\frac{1}{|V_i|}\frac{\partial |V_i|}{\partial |V_k|} + j\frac{\partial \theta_i}{\partial |V_k|})V_i, i \in \mathcal{N}.$$

The derived (4) is linear with respect to $\overline{W_{ik}}$ and W_{ik}. Similarly, (4) has a unique solution for a radial electrical network. Once $\overline{W_{ik}}$ and W_{ik} are obtained, the sensitivity coefficients with respect to the tap position of the transformer at Bus k are given by,

$$\frac{\partial |V_i|}{\partial |V_k|} = |V_i|\text{Re}(\frac{W_{ik}}{V_i}). \tag{5}$$

As the tap position of the transformers n_{tap} is an integer, the sensitivity coefficients to each tap change $\frac{\Delta |V_i|}{\Delta n_{\text{tap}}}$ can be calculated by,

$$\frac{\Delta |V_i|}{\Delta n_{\text{tap}}} = \frac{\partial |V_i|}{\partial |V_k|}\Delta V_{\text{tap}}, \tag{6}$$

where ΔV_{tap} is the voltage change per tap.

IV. DISCRETE MODELING OF VAR DEVICES

In this section, the discrete model of WTGs and SVCs/SVGs is described. It will be used as the prediction model for the MPC.

A. WTG modeling

As described in Section II, the Var reference for WTGs is Q_W^{ref}. Suppose the current time is t_0, $Q_W^{\text{ref}} = Q_W(t_0)+\Delta Q_W^{\text{ref}}$, where $Q_S(t_0)$ is the current Var measurement. The dynamic behaviour of the constant-Q control loop of WTGs can be described by a first order function,

$$\Delta Q_W = \frac{1}{1+sT_W}\Delta Q_W^{\text{ref}}, \tag{7}$$

where T_W is the time constant and s is the complex variable. The corresponding state space model is,

$$\Delta \dot{Q}_W = -\frac{1}{T_W}\Delta Q_W + \frac{1}{T_W}\Delta Q_W^{\text{ref}}. \tag{8}$$

The Var capabilities of modern WTGs (Type 3 and Type 4) Q_W are constrained by the operating limits of the converters [17]. For the full-converter WTGs (Type 4), the range of Var capability is larger because of the increased rating of the converter. The Var capability is dependent on the terminal voltage and active power P_W. A typical PQ curve of a full-converter WTG is illustrated in Fig. 3. Since P_W is assumed to be constant during the prediction horizon, the constraint of ΔQ_W can be determined according to $Q_W(t_0)$ and its PQ curve,

$$Q_W^{\text{min}} \leq \Delta Q_W + Q_W(t_0) \leq Q_W^{\text{max}}. \tag{9}$$

where Q_W^{min} and Q_W^{max} are the minimum and maximum Var capacity of WTG, respectively.
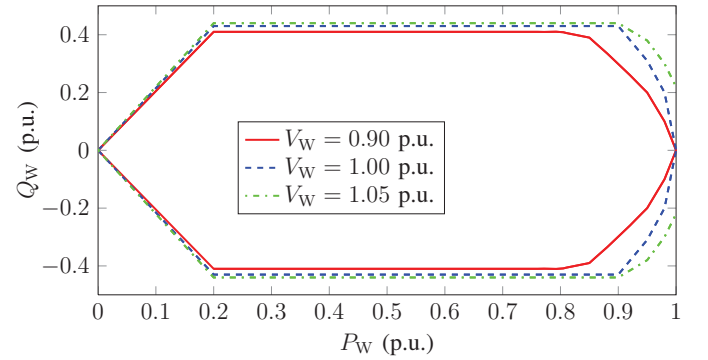

Fig. 3. PQ curve of a full-converter WTG.

B. SVC/SVG modeling

The voltage reference for SVCs/SVGs is V_S^{ref}, derived from the MPC controller. This reference value is then sent to the local PI controller and the equivalent Var reference Q_S^{ref} can be calculated by $Q_S^{\text{ref}} = Q_S(t_0) + \Delta Q_S^{\text{ref}}$, where

$$\Delta Q_S^{\text{ref}} = K_P(V_S^{\text{ref}} - V_S) + K_I\frac{1}{s}(V_S^{\text{ref}} - V_S), \tag{10}$$

where K_P and K_I are the proportional and integral gains of the PI controller, respectively.

The voltage at the controlled bus (POC) V_S is related to Q_S and Q_W. The sensitivity value is assumed to be constant during the prediction horizon, and

$$V_S = V_S(t_0) + \frac{\partial |V_S|}{\partial Q_S}\Delta Q_S + \frac{\partial |V_S|}{\partial Q_W}\Delta Q_W, \tag{11}$$

where $\frac{|\partial V_S|}{\partial Q_W}$ and ΔQ_W are the vectors including all WTGs.

The dynamic of the constant-Q control loop of SVC/SVG can be described by a first order function,

$$\Delta Q_S = \frac{1}{1+sT_S}\Delta Q_S^{\text{ref}}, \tag{12}$$

where T_S is the time constant and s is the complex variable.

With the following definitions,

$$\Delta V_{\mathrm{S}}^{\mathrm{ref}} \triangleq V_{\mathrm{S}}^{\mathrm{ref}} - V_{\mathrm{S}}(t_0), \tag{13}$$

$$\Delta V_{\mathrm{int}} \triangleq \frac{V_{\mathrm{S}}^{\mathrm{ref}} - V_{\mathrm{S}}}{s}, \tag{14}$$

where $\Delta V_{\mathrm{S}}^{\mathrm{ref}}$ indicates the reference of voltage change, ΔV_{int} is the integral of the deviation between $V_{\mathrm{S}}^{\mathrm{ref}}$ and V_{S} and s is the complex variable, (10)−(14) can be rewritten as the following state space form,

$$\begin{bmatrix} \Delta \dot{Q}_{\mathrm{S}} \\ \Delta \dot{V}_{\mathrm{int}} \end{bmatrix} = \boldsymbol{A_{\mathrm{S}}} \begin{bmatrix} \Delta Q_{\mathrm{S}} \\ \Delta V_{\mathrm{int}} \end{bmatrix} + \boldsymbol{E_{\mathrm{S}}} \Delta Q_{\mathrm{W}} + \boldsymbol{B_{\mathrm{S}}} \Delta V_{\mathrm{S}}^{\mathrm{ref}}, \tag{15}$$

with the following constraints,

$$Q_{\mathrm{S}}^{\mathrm{min}} \leq \Delta Q_{\mathrm{S}} + Q_{\mathrm{S}}(t_0) \leq Q_{\mathrm{S}}^{\mathrm{max}}, \tag{16}$$

$$V_{\mathrm{S}}^{\mathrm{min}} \leq V_{\mathrm{S}}^{\mathrm{ref}} \leq V_{\mathrm{S}}^{\mathrm{max}}, \tag{17}$$

where $Q_{\mathrm{S}}^{\mathrm{min}}$ and $Q_{\mathrm{S}}^{\mathrm{max}}$ are the minimum and maximum Var capacity of SVG, respectively; $V_{\mathrm{S}}^{\mathrm{min}}$ and $V_{\mathrm{S}}^{\mathrm{max}}$ are the minimum and maximum feasible voltages. More details of the derivation of (15) and mathematical expressions of $\boldsymbol{A_{\mathrm{S}}}$, $\boldsymbol{E_{\mathrm{S}}}$, $\boldsymbol{B_{\mathrm{S}}}$ are presented in Appendix.

C. General discrete model

Based on (8) and (15), the general state space model of continuous systems, including N_{S} SVCs/SVGs and N_{W} WTGs, can be formulated as,

$$\dot{x} = \boldsymbol{A}x + \boldsymbol{B}u \tag{18}$$

with

$$x = [\Delta Q_{\mathrm{S}_1}, \Delta V_{\mathrm{int}_1}, \cdots, \Delta Q_{\mathrm{S}_{N_{\mathrm{S}}}}, \Delta V_{\mathrm{int}_{N_{\mathrm{S}}}},$$
$$\Delta Q_{\mathrm{W}_1}, \cdots, \Delta Q_{\mathrm{W}_{N_{\mathrm{W}}}}]',$$
$$u = [\Delta V_{\mathrm{S}_1}^{\mathrm{ref}}, \cdots, \Delta V_{\mathrm{S}_{N_{\mathrm{S}}}}^{\mathrm{ref}}, \Delta Q_{\mathrm{W}_1}^{\mathrm{ref}}, \cdots, \Delta Q_{\mathrm{W}_{N_{\mathrm{W}}}}^{\mathrm{ref}}]',$$

$$\boldsymbol{A} = \left[\begin{array}{ccc|ccc} \boldsymbol{A_{\mathrm{S}_1}} & \cdots & 0 & \boldsymbol{E_{\mathrm{S}_1}} & \cdots & 0 \\ \vdots & \ddots & \vdots & \vdots & \ddots & \vdots \\ 0 & \cdots & \boldsymbol{A_{\mathrm{S}_{N_{\mathrm{S}}}}} & 0 & \cdots & \boldsymbol{E_{\mathrm{S}_{N_{\mathrm{W}}}}} \\ \hline 0 & \cdots & 0 & -\frac{1}{T_{\mathrm{W}_1}} & \cdots & 0 \\ \vdots & \ddots & \vdots & \vdots & \ddots & \vdots \\ 0 & \cdots & 0 & 0 & \cdots & -\frac{1}{T_{\mathrm{W}_{N_{\mathrm{W}}}}} \end{array}\right],$$

$$\boldsymbol{B} = \left[\begin{array}{ccc|ccc} \boldsymbol{B_{\mathrm{S}_1}} & \cdots & 0 & 0 & \cdots & 0 \\ \vdots & \ddots & \vdots & \vdots & \ddots & \vdots \\ 0 & \cdots & \boldsymbol{B_{\mathrm{S}_{N_{\mathrm{S}}}}} & 0 & \cdots & 0 \\ \hline 0 & \cdots & 0 & \frac{1}{T_{\mathrm{W}_1}} & \cdots & 0 \\ \vdots & \ddots & \vdots & \vdots & \ddots & \vdots \\ 0 & \cdots & 0 & 0 & \cdots & \frac{1}{T_{\mathrm{W}_{N_{\mathrm{W}}}}} \end{array}\right].$$

By applying the sampling time ΔT_{p}, according to the discretization method described in [18], (18) can be transformed to a discrete model,

$$x(k+1) = \boldsymbol{A_{\mathrm{d}}}x(k) + \boldsymbol{B_{\mathrm{d}}}u(k) \tag{19}$$

$$Q_{\mathrm{W}_i}^{\mathrm{min}} \leq \Delta Q_{\mathrm{W}_i}(k) + Q_{\mathrm{W}_i}(t_0) \leq Q_{\mathrm{W}_i}^{\mathrm{max}}, \; i \in [1, \cdots, N_{\mathrm{W}}]$$
$$Q_{\mathrm{S}_i}^{\mathrm{min}} \leq \Delta Q_{\mathrm{S}_i}(k) + Q_{\mathrm{S}_i}(t_0) \leq Q_{\mathrm{S}_i}^{\mathrm{max}}, \; i \in [1, \cdots, N_{\mathrm{S}}]$$
$$V_{\mathrm{S}_i}^{\mathrm{min}} \leq V_{\mathrm{S}_i}^{\mathrm{ref}}(k) \leq V_{\mathrm{S}_i}^{\mathrm{max}}, \; i \in [1, \cdots, N_{\mathrm{S}}]$$

where $\boldsymbol{A_{\mathrm{d}}}$, $\boldsymbol{B_{\mathrm{d}}}$ are the discrete forms of $\boldsymbol{A}$, $\boldsymbol{B}$ in (18), respectively.

V. COORDINATION WITH OLTC

As mentioned in Section II, the local automatic tap changer controller is included in the WFVC. Its working principle is illustrated in Fig. 4. In this controller, a deadband V_{DB} is introduced in order to avoid unnecessary switching around the reference voltage V_{ref}. Conventionally, V_{DB} is symmetrical around V_{ref}. Under a normal operating condition, the bus voltage V stays within the deadband. No actions are taken by the controller. At $t = t_{\mathrm{tri}}$, a timer is triggered. If this condition persists for longer than a preset time delay T_{delay}, the tap n_{tap} will increase ($n_{\mathrm{tap}} + 1$) or decrease ($n_{\mathrm{tap}} - 1$) according to the voltage condition [19]. T_{delay} is largely dependent on the tap changer design. A minimum of 2 seconds is given in [20]. The trigger time t_{tri} and tap position n_{tap} will be sent to the MPC controller.

For each control step, the MPC controller will check if there exists a potential tap action t_{act} within the prediction period T_{p}, indicated by $\mathrm{Sign_{tap}}$. Suppose the current time is $t = t_0$,

$$\mathrm{Sign_{tap}} = \begin{cases} 1, & \text{if } t_0 \leq t_{\mathrm{act}} \leq t_0 + T_{\mathrm{p}}. \\ 0, & \text{else.} \end{cases} \tag{20}$$

Once t_{act} is within $t_0 \sim t_0 + T_{\mathrm{p}}$ (Fig. 4), in the remaining of the prediction period $t_{\mathrm{act}} \sim t_0 + T_{\mathrm{p}}$, the tap change will occur. As the tap changer is located at the main transformer, which is the root bus of the collector system, the bus voltages along the feeders will be affected. The degree of the effect is related to the calculated sensitivity value $\frac{\Delta|V|}{\Delta n_{\mathrm{tap}}}$. It will be included in the calculation of the predicted voltages, which is described in the next section. Compared with the discrete or continuous modeling of OLTC in the MPC, this method is easier to be implemented without additional computation burden.
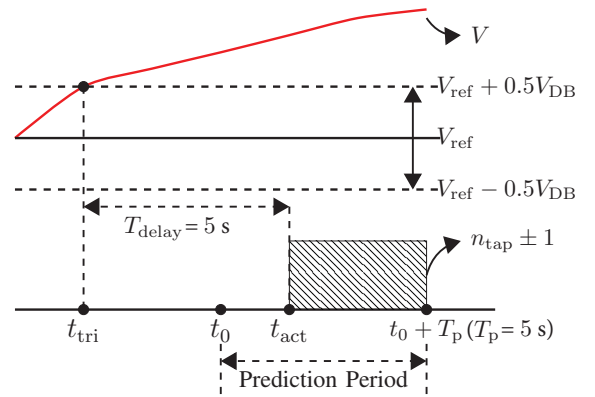

Fig. 4. Working princle of OLTC in MPC.

VI. MPC PROBLEM FORMULATION FOR WFVC

As described in Section II, two control modes are designed for different operating conditions. In this section, the cost

function as well as the constraints of the MPC based WFVC are formulated for both control modes.

To be noticed, the sampling period of the control action of the WFVC, ΔT_c, is normally in seconds, which is larger than the time constants of the fast Var devices, such as SVCs/SVGs. In order to better coordinate the fast and slow devices, the fast dynamics should also be captured. Therefore, the sampling period of the prediction, ΔT_p, is smaller. In this paper, ΔT_c is further divided into N_s steps. Accordingly, for a prediction horizon T_p, the number of control steps N_c can be calculated by $N_c = \frac{T_p}{\Delta T_c}$ and the total number of prediction steps can be calculated by $N_p = N_c \times N_s$.

The selection of the prediction horizon T_p is important for the control performance. If T_p is too small, the dynamics can't be well coordinated. If T_p is too large, the accuracy of the persistence assumption of P_W and sensitivity coefficients will decrease.

A. Corrective voltage control mode

If any bus voltage deviation of the wind farm violates its threshold, i.e. $\| V_{POC} - V_{POC}^{ref} \| \geq V_{POC}^{th}$ or $\| V_{MV} - V_{MV}^{ref} \| \geq V_{MV}^{th}$ or $\| V_W - V_W^{ref} \| \geq V_W^{th}$, the WFVC will be switched to this mode. V_{POC}, V_{MV} and V_W are the measured voltage at the POC, MV side of the main substation transformer and WTG buses, respectively. V_W is a vector, defined as $V_W = [V_{W_1}, V_{W_2}, \cdots]'$. V_{POC}^{ref} is the reference value derived from system operator (typically $1.0 \, \text{p.u.}$), V_W^{ref} is the nominal voltage of each WTG (typically $1.0 \, \text{p.u.}$), V_{POC}^{th} and V_W^{th} refer to the thresholds of V_{POC} and V_W, respectively. V_{POC}^{th} differs according to different grid codes. In this study, V_{POC}^{th} and V_{MV}^{th} are set $0.01 \, \text{p.u.}$ and $0.03 \, \text{p.u.}$, respectively. For V_W^{th}, since the protection configuration is usually set $[0.9, 1.1]$, to ensure sufficient operation margins, V_W^{th} is set 0.08. In order to differentiate the priority, the weighting factors for WTG voltages are larger.

1) Cost function: This control mode aims to ensure all the terminal voltages throughout the whole farm remain within the limits. The control inputs are ΔQ_W and V_S^{ref}. The cost function is expressed by,

$$\min_{\Delta Q_W, V_S^{ref}} \sum_{k=1}^{N_p} (\| \Delta V_{POC}^{pre}(k) \|_{W_{POC}}^2 + \| \Delta V_{MV}^{pre}(k) \|_{W_{MV}}^2 + \| \Delta V_W^{pre}(k) \|_{W_W}^2), \quad (21)$$

where $\Delta V_{POC}^{pre}(k)$, $\Delta V_{MV}^{pre}(k)$, $\Delta V_W^{pre}(k)$ are the deviations of V_{POC}, V_{MV} and V_W to their reference values at the prediction step k, respectively; W_{POC}, W_{MV} and W_W are the weighting factors. It should be noticed that only the buses with violated voltage are considered in the cost function. Before each formulation of the MPC problem, all the voltage deviations at the current time are calculated based on the measurements and their reference values. Once the voltage deviation is within the threshold, the corresponding penalty part will be neglected in the newly formulated MPC problem.

$\Delta V_{MV}^{pre}(k)$ and $\Delta V_W^{pre}(k)$ are affected by the Var injection of SVCs/SVGs, WTGs and tap change of OLTC, which can be calculated by,

$$\Delta V_{MV}^{pre}(k) = V_{MV} + \frac{\partial |V_{MV}|}{\partial Q_W} \Delta Q_W(k) + \frac{\partial |V_{MV}|}{\partial Q_S} \Delta Q_S(k) + \text{Sign}_{tap}(\frac{\Delta |V_{MV}|}{\Delta n_{tap}} \Delta n_{tap}) - V_{MV}^{ref}, \quad (22)$$

$$\Delta V_W^{pre}(k) = V_W + \frac{\partial |V_W|}{\partial Q_W} \Delta Q_W(k) + \frac{\partial |V_W|}{\partial Q_S} \Delta Q_S(k) + \text{Sign}_{tap}(\frac{\Delta |V_W|}{\Delta n_{tap}} \Delta n_{tap}) - V_W^{ref}. \quad (23)$$

Due to the electrical coupling with the external grid, the impact of the tap change at the V_{POC} is quite limited and neglected in this study. $\Delta V_{POC}^{pre}(k)$ can be obtained by,

$$\Delta V_{POC}^{pre}(k) = V_{POC} + \frac{\partial |V_{POC}|}{\partial Q_W} \Delta Q_W(k) + \frac{\partial |V_{POC}|}{\partial Q_S} \Delta Q_S(k) - V_{POC}^{ref}. \quad (24)$$

2) Constraints: Besides (19), the other constraints are,
If $\| V_{POC} - V_{POC}^{ref} \| \leq V_{POC}^{th}$,

$$-V_{POC}^{th} \leq \Delta V_{POC}^{pre}(k) \leq V_{POC}^{th}. \quad (25)$$

If $\| V_{MV} - V_{MV}^{ref} \| \leq V_{MV}^{th}$,

$$-V_{MV}^{th} \leq \Delta V_{MV}^{pre}(k) \leq V_{MV}^{th}. \quad (26)$$

If $\| V_W - V_W^{ref} \| \leq V_W^{th}$,

$$-V_W^{th} \leq \Delta V_W^{pre}(k) \leq V_W^{th}. \quad (27)$$

The constraints $(25)-(27)$ are conditional. Once the voltage violates the constraint, in order to guarantee a feasible solution of the MPC, this constraint needs to be relaxed and thus removed in this case.

Since the control inputs could only be changed at the control points, the values within the control period are maintained:

$$\Delta Q_W(iN_s + k) = \Delta Q_W(iN_s), \quad (28)$$
$$V_S^{ref}(iN_s + k) = V_S^{ref}(iN_s), \quad (29)$$
$$i \in [0, \cdots N_p - 1], k \in [0, \cdots N_s - 1].$$

B. Preventive voltage control mode

If all the bus voltage deviations are within their thresholds, the WFVC will be switched to the preventive control mode.

1) Cost function: The control objective of this mode is twofold. Firstly, in order to deal with the potential disturbance in the future, the fast dynamic Var support capabilities shall be maximized. It can be realized by minimizing the Q_S to its middle level of the operating range $\frac{1}{2}(Q_S^{max} - Q_S^{min})$. The reduced Q_S will be substituted by other slower Var sources for maintaining the voltage of buses throughout the wind farm. Secondly, in order to better fulfill the requirement from the system operator, the deviation between the measured voltage at POC V_{POC} and its reference value will be further minimized. The cost function is expressed by,

$$\min_{\Delta Q_W, V_S^{ref}} \sum_{k=1}^{N_p} (\| \Delta V_{POC}^{pre}(k) \|_{W_{POC}}^2 + \| \Delta Q_S^{pre}(k) \|_{W_S}^2), \quad (30)$$

where $\Delta Q_{\mathrm{S}}^{\mathrm{pre}}(k)$ is the deviation of Q_{S} from its middle operating level at the prediction step k, W_{S} refers to its weighting factor, $\Delta Q_{\mathrm{S}}^{\mathrm{pre}}(i)$ is calculated by,

$$\Delta Q_{\mathrm{S}}^{\mathrm{pre}}(k) = Q_{\mathrm{S}} + \Delta Q_{\mathrm{S}}(k) - \frac{1}{2}(Q_{\mathrm{S}}^{\mathrm{max}} - Q_{\mathrm{S}}^{\mathrm{min}}). \quad (31)$$

2) Constraints: The constraints of this mode are similar to those of the corrective control mode.

When the WFVC switches between these two modes, the chattering may occur. In order to prevent the chattering, a hysteresis loop can be used.

The formulated MPC problem can be transformed to a standard Quadratic Programming (QP) problem, which can be efficiently solved by commercial QP solvers in milliseconds [21].

VII. CASE STUDY

In this section, a wind farm, comprised of $20 \times 5\,\mathrm{MW}$ full-converter WTGs, $1 \times \pm 7\,\mathrm{MVar}$ SVG and $1 \times$ OLTC with $\pm 8 \times 1.25\%$ tap changer, was used for the case study. Its configuration is shown in Fig. 1. The wind farm is integrated into the Nordic 32 system model, developed by CIGRÉ [22]. The connected bus is Bus 1042, which is located at the terminal of the grid, as shown in Fig. 5. The wind field modeling considering turbulences and wake effects for the wind farm was generated from SimWindFarm [23], a toolbox for dynamic wind farm model, simulation and control.

Two scenarios were selected to test the efficacy of the proposed WFVC. Firstly, the wind farm operates under normal operation. The internal wind power fluctuation was considered. Secondly, besides the internal power fluctuation, the impact of the external grid on the wind farm was taken into account. In both scenarios, the results of the Optimal Controller (OPT) based on the current measurement was compared with those of proposed MPC controller.

The sampling periods of the WFVC ΔT_{c}, the prediction horizon ΔT_{p} were set as $1\,\mathrm{s}$ and $0.2\,\mathrm{s}$, respectively. The prediction horizon T_{p} was set as $T_{\mathrm{p}} = 5\,\mathrm{s}$.

A. Normal operation

In real operation, the wind farm is required to have the capability to limit the power production ramp rate by many system operators in order to smooth out the wind power variation [24]. In this paper, the ramp rate control is applied in the wind farm controller. The maximum ramp rate is set 10% of the installed capacity per minute ($10\,\mathrm{MW/min}$ for this case). The simulation time is $600\,\mathrm{s}$. The total power output of the wind farm P_{WF} is shown in Fig. 6.

As mentioned before, the fluctuation of active power has an impact on the prediction accuracy of P_{W} and may further affect the control performance. In order to sufficiently test the proposed WFVC, different wind power conditions should be included. In this study, the whole operation period is divided into two parts. During $0 \sim 350\,\mathrm{s}$, the wind power fluctuates between $50\,\mathrm{MW}$ and $70\,\mathrm{MW}$. During $100 \sim 200\,\mathrm{s}$, the wind power output becomes smoother, which fluctuates between $70\,\mathrm{MW}$ and $76\,\mathrm{MW}$.
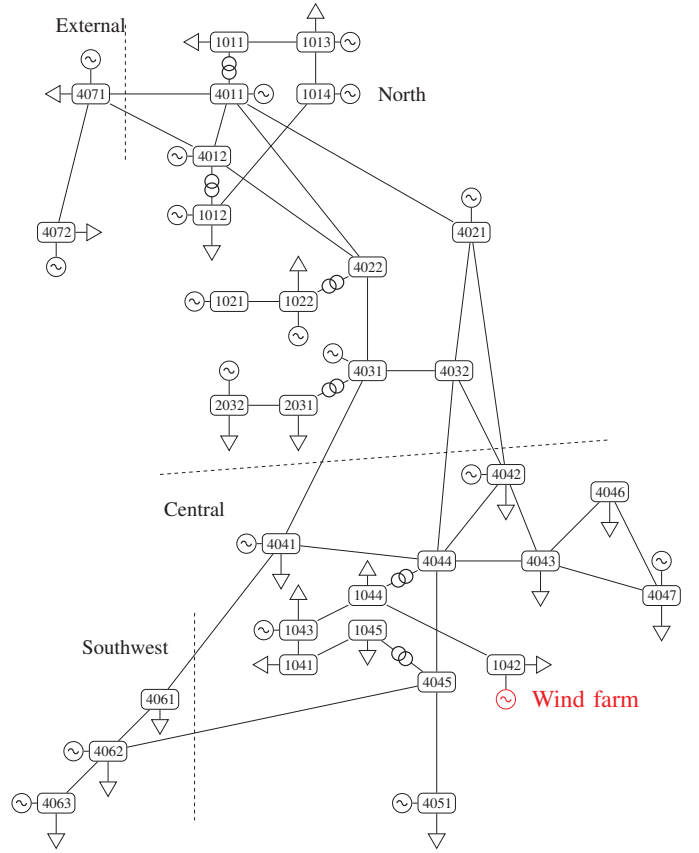

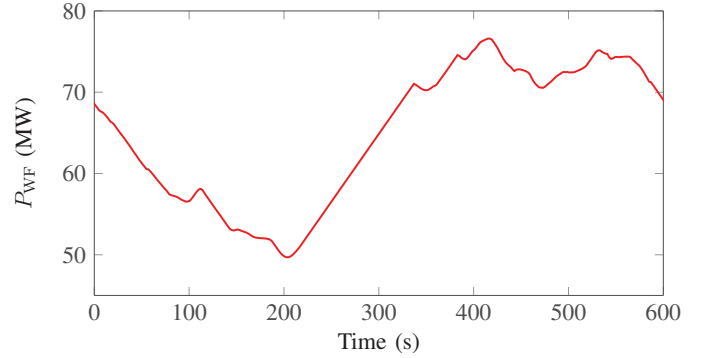Fig. 5. Nordic 32 system with wind farm.

Fig. 6. Power output of the wind farm.

As the furthest bus along the feeder, WT07 is chosen as the representative WTG bus (see Fig. 1). The simulation results of voltages at three important buses: V_{POC}, V_{MV} and V_{W_7} are shown in Fig. 7. All the voltage deviations are within their thresholds and therefore the WFVC operates in the preventive control mode.

As the primary control objective of this mode, it can be observed V_{POC} is regulated around its reference value $V_{\mathrm{POC}}^{\mathrm{ref}} = 1\,\mathrm{p.u.}$ (see Fig. 7(a)). Only very small deviations are detected when P_{WF} is close to the wind farm capacity or when power fluctuates strongly. For the former case, since P_{W} is almost the maximum output, the Var contribution of WTGs are limited (see Fig. 3). For the latter case, the fast variation of P_{W} has an impact on the voltage deviation. However, the standard
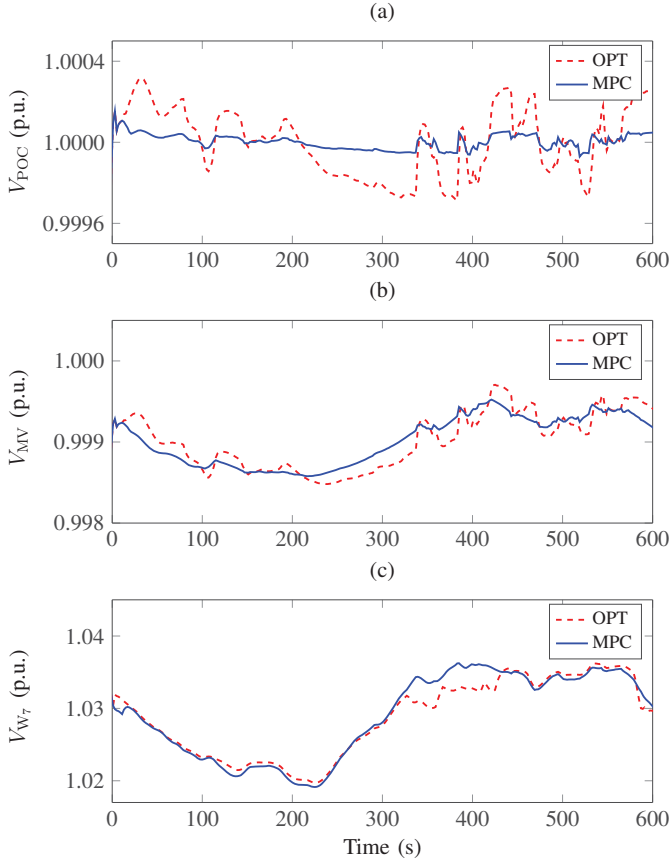
Fig. 7.   Voltages of different buses within the wind farm.

deviation $\sigma(V_{\text{POC}})$ of both controllers are quite small: 0.017% for OPT and 0.0030% for MPC. Both controllers show good control performances. Comparably, the performance of MPC is better.

As the other control objective of this mode, the simulation results of Q_{S} of both controllers are shown in Fig. 8. Only small Q_{S} are detected for both controllers. In other words, the fast Var reserve has been maximized. Both controllers show good control performances. The mean value $\bar{Q}_{\text{S}}$ and standard deviation $\sigma(Q_{\text{S}})$ are 0.01% and 0.57% for OPT. For MPC, $\bar{Q}_{\text{S}}$ and $\sigma(Q_{\text{S}})$ are 0.00% and 0.09%, respectively. Comparably, the performance of MPC is better.
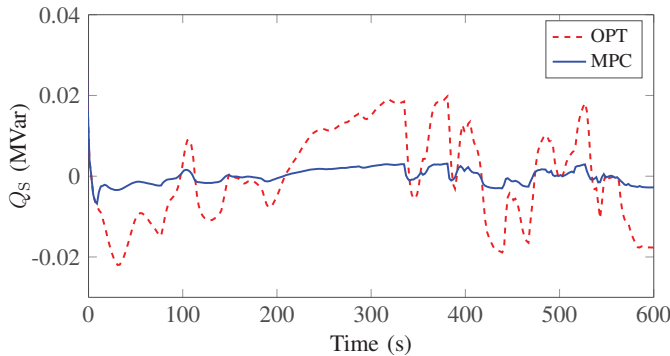

Fig. 8.   Reactive power of the SVG Q_{S}.

B. Operation with LVRT

In this case, the disturbances of the external grid are considered. A three-phase short-circuit event at Bus 1044 is used to represent the fault condition. The event occurs at $t = 20\,\text{s}$ and it is cleared at $t = 20.2\,\text{s}$. The simulation time is $70\,\text{s}$. The simulation results are illustrated in Figs. 9-13.
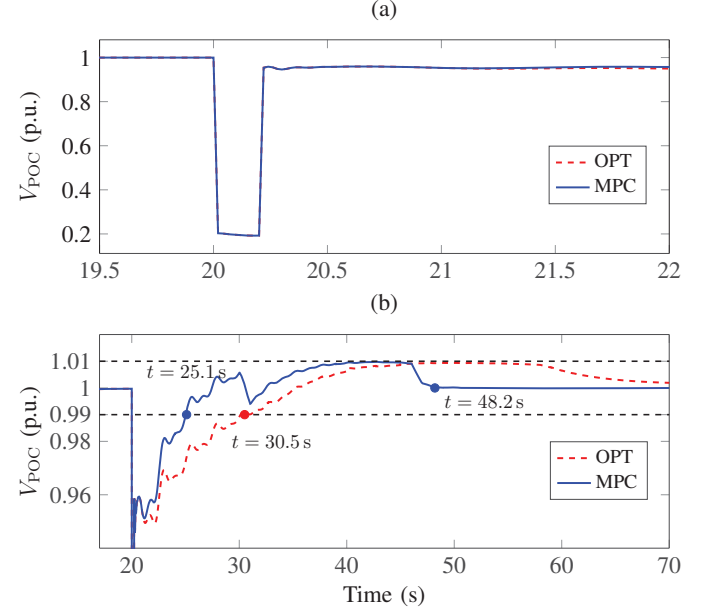

Fig. 9.   Voltage of POC, (a) zoomed part in time axis, (b) zoomed part in voltage axis.
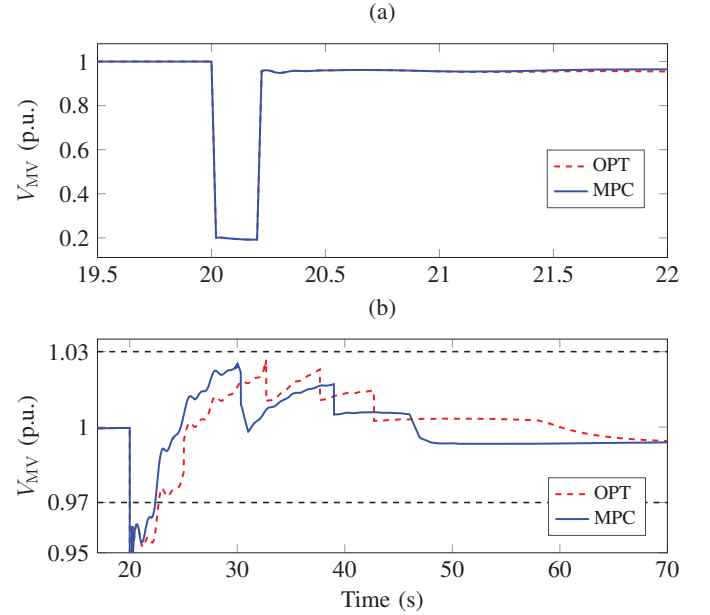

Fig. 10.   Voltage of MV, (a) zoomed part in time axis, (b) zoomed part in voltage axis.

During $20 \sim 20.2\,\text{s}$, the short-circuit fault results in a sudden decreases of V_{POC}, V_{MV} and V_{W}, which violate their thresholds (Figs. 9(a)-11(a)). The WFVC switches to the corrective control mode. Since the control period of the
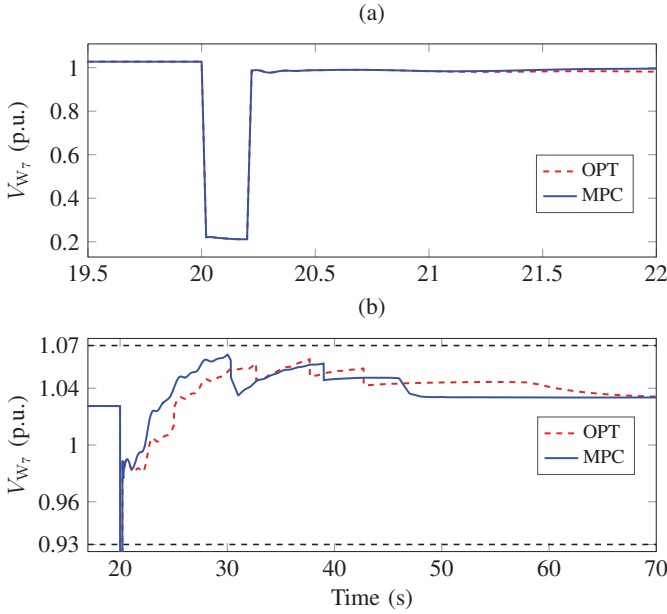
Fig. 11. Voltage of WT07, (a) zoomed part in time axis, (b) zoomed part in voltage axis.

WFVC is $1\,\mathrm{s}$, the fault is within the interval between two control actions ($20 \sim 21\,\mathrm{s}$). The SVG starts compensating the reactive power independently, as shown in Fig. 12. Due to the large voltage drop, Q_S reaches to its capacity limit Q_S^{max} immediately. After the fault, the voltages start recovering.
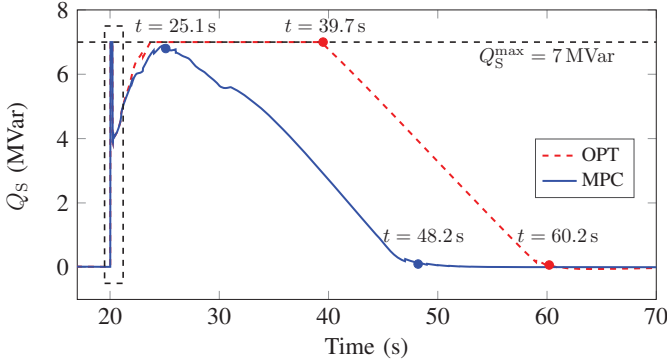

Fig. 12. Reactive power of the SVG Q_S.

For the OPT, the recovery is slow. V_{W_7} goes back to its threshold shortly after the fault (Fig. 11(b)). Subsequently, V_{MV} returns within its thresholds at about $t = 22.8\,\mathrm{s}$ (Fig. 10(b)). ΔV_{POC} returns within its threshold at $t = 30.5\,\mathrm{s}$ (Fig. 9(b)). Accordingly, the WFVC switches back to the preventive control mode. Then V_{POC} is controlled to move back to its reference ($1\,\mathrm{p.u.}$). This process is slow and lasts until the end of the simulation ($t = 70\,\mathrm{s}$). During the voltage recovery, the Var injection Q_S has reached to its maximum capacity ($Q_S^{max} = 7\,\mathrm{MVar}$) and stays at this value until $t = 39.7\,\mathrm{s}$, as shown in Fig. 12. It means that the SVG can't provide fast dynamic Var support for possible voltage drop during that period. After $t = 39.7\,\mathrm{s}$, Q_S starts decreasing and reduces to around $0\,\mathrm{MVar}$ at $t = 60.2\,\mathrm{s}$. Four tap actions are detected at $t = t_1$, $t = t_2$, $t = t_3$ and $t = t_4$, respectively (Fig. 13).
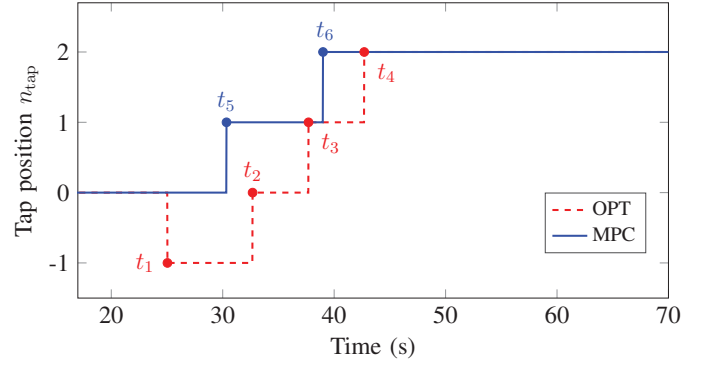

Fig. 13. Tap position of OLTC at the main substation.

For the MPC, the recovery is much faster. As shown in Fig. 11(b) and Fig. 10(b), V_{W_7} and V_{MV} go back to be within their thresholds shortly after the fault. Subsequently, V_{POC} returns to be within its threshold at $t = 25.1\,\mathrm{s}$ (Fig. 9(b)). Accordingly, the WFVC switches back to the preventive control mode. V_{POC} is then controlled to move back to its reference ($1\,\mathrm{p.u.}$). This process is fast and finished at $t = 48.2\,\mathrm{s}$. During the voltage recovery, Q_S doesn't reach to Q_S^{max}. After $t = 25.1\,\mathrm{s}$, Q_S starts decreasing and gets to around $0\,\mathrm{MVar}$ at $t = 48.2\,\mathrm{s}$, which is much earlier than that of the OPT. Two tap actions are detected at $t = t_5$ and $t = t_6$, respectively (Fig. 13).

It should be noted that the tested wind farm was based on full-converter WTGs (Type 4). As mentioned in Section IV-A, both Type 3 and Type 4 WTGs have Var regulation capability. Comparatively, the Var capacity of Type 3 WTGs is smaller. Accordingly, the capability to support voltage at the collector bus or at the POC is smaller. Since the proposed MPC can efficiently coordinate between the multiple Var devices, the control performance with Type 3 WTGs can be guaranteed when the Var reserve is sufficient. However, for the case when a large amount of Var is required and the reserve is insufficient, such as severe disturbance in the external grid, the control performance with Type 3 WTGs may be worse than that with Type 4 WTGs and the capacity of the Var compensation devices shall be increased.

VIII. CONCLUSION

In this paper, the MPC based WFVC is developed to optimally coordinate the Var/Volt regulation devices with different time constants. Two control modes are designed for the voltage violated and normal operation conditions. For the corrective voltage control mode, besides the voltage at the POC, the other terminal voltages throughout the whole wind farm are regulated to be within the limits. For the preventive voltage control mode, the dynamic Var support capabilities are maximized to prevent the potential disturbance and the voltage of the POC is further improved to better fulfill the requirement from the system operator. In order to improve the computation efficiency, the analytical method is used to calculate the sensitivity coefficients. The case studies show the proposed MPC has better control performances compared with the conventional optimal controller, especially under disturbances.

APPENDIX

The derivation of the state space model of SVC/SVG for the proposed WFVC can be divided into three steps.

Step 1: Calculation of $\Delta Q_{\mathrm{S}}^{\mathrm{ref}}$.

Based on (11) and (14), (10) can be transformed into,

$$\Delta Q_{\mathrm{S}}^{\mathrm{ref}} = K_{\mathrm{P}}(V_{\mathrm{S}}^{\mathrm{ref}} - V_{\mathrm{S}}) + K_{\mathrm{I}}\frac{1}{s}(V_{\mathrm{S}}^{\mathrm{ref}} - V_{\mathrm{S}}) \tag{32}$$

$$= K_{\mathrm{P}}(V_{\mathrm{S}}^{\mathrm{ref}} - V_{\mathrm{S}}(t_0) - \frac{\partial |V_{\mathrm{S}}|}{\partial Q_{\mathrm{S}}}\Delta Q_{\mathrm{S}} - \frac{\partial |V_{\mathrm{S}}|}{\partial Q_{\mathrm{W}}}\Delta Q_{\mathrm{W}})$$
$$+ K_{\mathrm{I}}\Delta V_{\mathrm{int}}.$$

Substitute (13) into (32),

$$\Delta Q_{\mathrm{S}}^{\mathrm{ref}} = K_{\mathrm{P}}(\Delta V_{\mathrm{S}}^{\mathrm{ref}} - \frac{\partial |V_{\mathrm{S}}|}{\partial Q_{\mathrm{S}}}\Delta Q_{\mathrm{S}} - \frac{\partial |V_{\mathrm{S}}|}{\partial Q_{\mathrm{W}}}\Delta Q_{\mathrm{W}}) \tag{33}$$
$$+ K_{\mathrm{I}}\Delta V_{\mathrm{int}}.$$

Step 2: Derivation of the differential equation of ΔQ_{S}.

The equation (12) can be transformed into the following differential equation,

$$\Delta \dot{Q}_{\mathrm{S}} = -\frac{1}{T_{\mathrm{S}}}\Delta Q_{\mathrm{S}} + \frac{1}{T_{\mathrm{S}}}\Delta Q_{\mathrm{S}}^{\mathrm{ref}}, \tag{34}$$

Substitute (33) into (34),

$$\Delta \dot{Q}_{\mathrm{S}} = -\frac{1}{T_{\mathrm{S}}}(1 + \frac{K_{\mathrm{P}}}{T_{\mathrm{S}}}\frac{\partial |V_{\mathrm{S}}|}{\partial Q_{\mathrm{S}}})\Delta Q_{\mathrm{S}} + \frac{K_{\mathrm{I}}}{T_{\mathrm{S}}}\Delta V_{\mathrm{int}} \tag{35}$$
$$- \frac{K_{\mathrm{P}}}{T_{\mathrm{S}}}\frac{\partial |V_{\mathrm{S}}|}{\partial Q_{\mathrm{W}}}\Delta Q_{\mathrm{W}} + \frac{K_{\mathrm{P}}}{T_{\mathrm{S}}}\Delta V_{\mathrm{S}}^{\mathrm{ref}}.$$

Step 3: Derivation of the differential equation of ΔV_{int}.

The equation (14) can be transformed into the following differential equation,

$$\Delta \dot{V}_{\mathrm{int}} = (V_{\mathrm{S}}^{\mathrm{ref}} - V_{\mathrm{S}}). \tag{36}$$

Substitute (11) and (13) into (36),

$$\Delta \dot{V}_{\mathrm{int}} = (V_{\mathrm{S}}^{\mathrm{ref}} - V_{\mathrm{S}}) \tag{37}$$
$$= V_{\mathrm{S}}^{\mathrm{ref}} - V_{\mathrm{S}}(t_0) - \frac{\partial |V_{\mathrm{S}}|}{\partial Q_{\mathrm{S}}}\Delta Q_{\mathrm{S}} - \frac{\partial |V_{\mathrm{S}}|}{\partial Q_{\mathrm{W}}}\Delta Q_{\mathrm{W}}$$
$$= \Delta V_{\mathrm{S}}^{\mathrm{ref}} - \frac{\partial |V_{\mathrm{S}}|}{\partial Q_{\mathrm{S}}}\Delta Q_{\mathrm{S}} - \frac{\partial |V_{\mathrm{S}}|}{\partial Q_{\mathrm{W}}}\Delta Q_{\mathrm{W}}.$$

Based on (35) and (37), the state space model of SVC/SVG can be derived,

$$\begin{bmatrix} \Delta \dot{Q}_{\mathrm{S}} \\ \Delta \dot{V}_{\mathrm{int}} \end{bmatrix} = \boldsymbol{A_{\mathrm{S}}}\begin{bmatrix} \Delta Q_{\mathrm{S}} \\ \Delta V_{\mathrm{int}} \end{bmatrix} + \boldsymbol{E_{\mathrm{S}}}\Delta Q_{\mathrm{W}} + \boldsymbol{B_{\mathrm{S}}}\Delta V_{\mathrm{S}}^{\mathrm{ref}}, \tag{38}$$

where

$$\boldsymbol{A_{\mathrm{S}}} = \begin{bmatrix} -\frac{1}{T_{\mathrm{S}}}(1 + K_{\mathrm{P}}\frac{\partial |V_{\mathrm{S}}|}{\partial Q_{\mathrm{S}}}) & \frac{K_{\mathrm{I}}}{T_{\mathrm{S}}} \\ -\frac{\partial |V_{\mathrm{S}}|}{\partial Q_{\mathrm{S}}} & 0 \end{bmatrix},$$

$$\boldsymbol{E_{\mathrm{S}}} = \begin{bmatrix} -\frac{K_{\mathrm{P}}}{T_{\mathrm{S}}}\frac{\partial |V_{\mathrm{S}}|}{\partial Q_{\mathrm{W}}} \\ -\frac{\partial |V_{\mathrm{S}}|}{\partial Q_{\mathrm{W}}} \end{bmatrix}, \boldsymbol{B_{\mathrm{S}}} = \begin{bmatrix} \frac{K_{\mathrm{P}}}{T_{\mathrm{S}}} \\ 1 \end{bmatrix}.$$

REFERENCES

[1] M. J. Hossain, H. R. Pota, M. A. Mahmud, and R. Ramos, "Investigation of the impacts of large-scale wind power penetration on the angle and voltage stability of power systems," *IEEE Syst. Journal*, vol. 6, no. 1, pp. 76–84, 2012.

[2] T. Neumann, C. Feltes, and I. Erlich, "Response of DFG-based wind farms operating on weak grids to voltage sags," in *Proc. Power Eng. Soc. Gen. Meeting*, 2011, pp. 1–6.

[3] Q. Wu, Z. Xu, and J. Østergaard, "Grid integration issues for large scale wind power plants," in *Proc. Power Eng. Soc. Gen. Meeting*, 2010, pp. 1–6.

[4] Z. Chen, J. M. Guerrero, and F. Blaabjerg, "A review of the state of the art of power electronics for wind turbines," *IEEE Trans. Power Electron.*, vol. 24, no. 8, pp. 1859–1875, 2009.

[5] J. Fortmann, M. Wilch, F. W. Koch, and I. Erlich, "A novel centralised wind farm controller utilising voltage control capability of wind turbines," in *PSCC Power Syst. Comput. Conf.*, 2008.

[6] D. Jovcic and K. Ahmed, *High Voltage Direct Current Transmission: Converters, Systems and DC Grids*. John Wiley & Sons, 2015.

[7] E. V. Larsen and A. S. Achilles, "System and method for voltage control of wind generators," Sep. 5 2013, US Patent App. 14/018,482.

[8] N. Efkarpidis, C. Gonzalez de Miguel, T. Wijnhoven, D. Van Dommelen, T. De Rybel, and J. Driesen, "Technical assessment of on-load tap-changers in flemish LV distribution grids," in *Proc. 3rd edition Solar Integration Workshop*, pp. 94–101, 2013.

[9] P. E. Sørensen, A. D. Hansen, F. Iov, F. Blaabjerg, and M. H. Donovan, "Wind farm models and control strategies," Risø National Laboratory, Roskilde, Tech. Rep.Risø-4-1464, Aug. 2005.

[10] A. D. Hansen, P. E. Sørensen, F. Iov, and F. Blaabjerg, "Centralised power control of wind farm with doubly fed induction generators," *Renewable Energy*, vol. 31, no. 7, pp. 935–951, 2006.

[11] B. Karthikeya and R. Schutt, "Overview of wind park control strategies," *IEEE Trans. Sustain. Energy*, vol. 5, no. 2, pp. 416–422, Apr. 2014.

[12] Q. Guo, H. Sun, B. Wang, B. Zhang, W. Wu, and L. Tang, "Hierarchical automatic voltage control for integration of large-scale wind power: Design and implementation," *Electric Power Systems Research*, vol. 120, pp. 234–241, 2015.

[13] M. Wang-Hansen, R. Josefsson, and H. Mehmedovic, "Frequency controlling wind power modeling of control strategies," *IEEE Trans. Sustain. Energy*, vol. 4, no. 4, pp. 954–959, 2013.

[14] D. K. Khatod, V. Pant, and J. Sharma, "A novel approach for sensitivity calculations in the radial distribution system," *IEEE Trans. Power Del.*, vol. 21, no. 4, pp. 2048–2057, 2006.

[15] M. Haque, "A general load flow method for distribution systems," *Electric Power Systems Research*, vol. 54, no. 1, pp. 47–54, 2000.

[16] K. Christakou, J. LeBoudec, M. Paolone, and D.-C. Tomozei, "Efficient computation of sensitivity coefficients of node voltages and line currents in unbalanced radial electrical distribution networks," *IEEE Trans. Smart Grid*, vol. 4, no. 2, pp. 741–750, 2013.

[17] H. Amaris, M. Alonso, and C. A. Ortega, *Reactive Power Management of Power Networks with Wind Generation*. Springer Science & Business Media, 2012.

[18] R. Tóth, *Modeling and identification of linear parameter-varying systems*. Springer, 2010.

[19] Y. N. N. Tchokonte, *Real-time identification and monitoring of the voltage stability margin in electric power transmission systems using synchronized phasor measurements*. Kassel university press GmbH, 2009.

[20] K. M. Muttaqi, A. D. Le, M. Negnevitsky, and G. Ledwich, "A coordinated voltage control approach for coordination of oltc, voltage regulator, and dg to regulate voltage in a distribution feeder," *IEEE Trans. Ind. Appl.*, vol. 51, no. 2, pp. 1239–1248, 2015.

[21] H. J. Ferreau, "Model predictive control algorithms for applications with millisecond timescales," Ph.D. dissertation, PhD thesis, KU Leuven, 2011.

[22] K. Walve, "Nordic32a–a CIGRÉ test system for simulation of transient stability and long term dynamics," Stockholm, Sweden: Svenska Kraftnät, 1994.

[23] J. D. Grunnet, M. Soltani, T. Knudsen, M. Kragelund, and T. Bak, "Aeolus toolbox for dynamic wind farm model, simulation and control," in *Proc. of the 2010 European Wind Energy Conf.*, 2010.

[24] B. Fox, *Wind power integration: connection and system operational aspects*. IET, 2007.